Passivating the sulfur vacancy in monolayer MoS_2

Haichang Lu, Andrew Kummel, and John Robertson

Citation: APL Materials **6**, 066104 (2018); doi: 10.1063/1.5030737
View online: https://doi.org/10.1063/1.5030737
View Table of Contents: http://aip.scitation.org/toc/apm/6/6
Published by the American Institute of Physics

APL MATERIALS **6**, 066104 (2018)

Passivating the sulfur vacancy in monolayer MoS_2

Haichang Lu,[1] Andrew Kummel,[2] and John Robertson[1,a]
[1]*Department of Engineering, Cambridge University, Cambridge CB2 1PZ, United Kingdom*
[2]*Department of Chemistry and Biochemistry, UC, San Diego, California 92093, USA*

(Received 25 March 2018; accepted 30 May 2018; published online 12 June 2018)

Various methods to passivate the sulfur vacancy in 2D MoS_2 are modeled using density functional theory (DFT) to understand the passivation mechanism at an atomic scale. First, the organic super acid, bis(trifluoromethane)sulfonimide (TFSI) is a strong protonating agent, and it is experimentally found to greatly increase the photoluminescence efficiency. DFT simulations find that the effectiveness of passivation depends critically on the charge state and number of hydrogens donated by TFSI since this determines the symmetry of the defect complex. A symmetrical complex is formed by three hydrogen atoms bonding to the defect in a −1 charge state, and this gives no bandgap states and a Fermi level in the midgap. However, a charge state of +1 gives a lower symmetry complex with one state in the gap. One or two hydrogens also give complexes with gap states. Second, passivation by O_2 can provide partial passivation by forming a bridge bond across the S vacancy, but it leaves a defect state in the lower bandgap. On the other hand, substitutional additions do not shift the vacancy states out of the gap. https://doi.org/10.1063/1.5030737

2D semiconductors such as the transition metal dichalcogenides (TMDs) have attracted considerable attention as opto-electronic devices because of their direct bandgap in their monolayer form[1–3] and as alternatives to Si and III-Vs in field effect transistors (FETs) because their thin layers allow excellent electrostatic control of their channels, and so their FETs give good short channel performance.[4,5] Their wide range of bandgaps and band offsets give them the potential for use as tunnel field effect transistors.[6,7] Their interlayer van der Waals bonding means that the pristine systems in principle have no dangling bonds. However, a large concentration of defects (~10^{13} cm^{-3}), thought to be sulfur vacancies, is seen in transmission electron microscopy and scanning tunneling microscopy (STM) on exfoliated samples,[8,9] and many like-atom bonds exist at the grain boundaries in samples grown by chemical vapor deposition (CVD).[10,11] Both types of defects will give rise to gap states and will reduce the device performance. For example, sulfur vacancies are seen to reduce the photoluminescence efficiencies by typically 10^4,[12] while their field-effect mobility in devices is well below their phonon limited mobility[13] due to both high contact resistances[14] and defects.

In 3D semiconductors, there are strategies available to passivate defects. In MoS_2, ways to passivate defects have been tried with varying success, but there is presently no general understanding of how best to achieve this. The most successful passivation process so far has been treating the sample by an organic superacid bis(trifluoromethane) sulfonamide (TFSI).[12] In this paper, we study various possible passivation schemes for TMDs and explain why they are more complicated than for simpler covalent semiconductors like Si.

Several passivation schemes for MoS_2 have been reported. (1) MoS_2 defect states can be removed by charge transfer doping via the van der Waals bonding of an organic monolayer, titanyl phthalocyanine (TiOPC).[15] (2) Thiol-based molecules can reduce the sulfur vacancy density on MoS_2 and

[a]Author to whom correspondence should be addressed: jr@eng.cam.ac.uk

achieve a high mobility of 80 cm^2/(V s) by a series of sulfurization reactions.[16,17] Chemisorbed thiol groups can also achieve *p*-type or *n*-type doping by choosing different functional groups.[18,19] (3) Molecular oxygen can passivate MoS_2 via chemisorption at the sulfur vacancy site.[20] This removes some vacancy gap states[21] and allows the photoluminescence (PL) efficiency to recover.[22] (4) Monolayer MoS_2 can be treated with the organic super acid TFSI. This improves the PL quantum yield and efficiency.[12,23–25]

Passivation can be defined as a process removing all defect states from the gap while allowing the Fermi energy E_F to return to the midgap. There are two standard methods to passivate defects in 3D semiconductors. (1) Use a chemical reactant which bonds strongly with the defect so that the resulting electronic states now lie outside the gap.[26–28] (2) Shift the defect states away from the relevant energy range.[29–31] Examples of the first method are the passivation of the residual Si dangling bonds at the Si/SiO_2 interface by hydrogen, where the resulting Si—H bonding and antibonding states lie in the valence band (VB) and conduction band (CB) respectively.[27] Examples of the second method are adding InP capping layers to the active InGaAs channel layer, where the surface states of the InP layers lie outside the energy range of the InGaAs bandgap, while the original InGaAs gap states now form bulk bonds with states outside its bandgap.[30,31]

We now use a series of defect supercell calculations to investigate possible defect reactions. The atomic geometries and electronic properties of three passivation schemes are calculated using the density functional theory (DFT) plane-wave CASTEP code.[32,33] Ultra-soft pseudopotentials with a plane-wave cut-off energy of 320 eV are used. The Perdew-Burke-Ernzerhof (PBE) form of the generalized gradient approximation (GGA) is used as the electron exchange-correlation functional. The GGA treatment of the van der Waals interaction is corrected using the Grimme scheme.[34] Geometry relaxation is performed until the residue force is lower than 0.03 eV/Å. A convergence test finds that a $4 \times 4 \times 1$ supercell with a vacuum gap of 30 Å and a $3 \times 3 \times 1$ k-point mesh describe well the 2D system with a single sulfur vacancy. To overcome the error caused by the periodical mirror charge, a self-consistent dipole correction is implemented. Spin-polarization is used for molecular oxygen. Although molecular oxygen is a spin triplet, when it bonds onto the sulfur vacancy it becomes a singlet state.

The defect formation energies are calculated using the supercell method. Corrections for defect charges and band occupations are applied as in the Lany and Zunger scheme.[35] The total energy of the perfect host supercell (E_H) and the supercell with defect (E_q) are calculated for different charge states. The defect formation energy H_q is then found from

$$H_q(E_F, \mu) = [E_q - E_H] + q(E_V + \Delta E_F) + \sum_{\alpha} n_\alpha(\mu_\alpha^0 + \Delta\mu_\alpha), \quad (1)$$

where q is the charge on the system and E_q is the energy of charged system with a defect. E_H is the energy of the charged defect-free system, E_V is the valence band maximum (VBM), and ΔE_F is the Fermi level with the respect to VBM. n_α is the number of atoms of species α, and μ_α is the relative chemical potential of the element α.

The equilibrium lattice parameter of 2D MoS_2 is calculated in GGA to be 3.17 Å, a 0.7% error compared to the experimental value.[36] The calculated GGA bandgap is 1.72 eV compared to an experimental optical bandgap of 1.80 eV[1] and a calculated bandgap of 1.88 eV in screened exchange (sX).[37] Thus, GGA gives less bandgap error for MoS_2 than for other layered chalcogenides like HfS_2 or InSe.[38]

For the defects, TFSI is known to greatly improve the PL efficiency.[12] It is dissolved in an organic alkane forming the TFSI anion and a nearly-free proton which can hop from anion to anion.[39] The TFSI anion is physisorbed near the S vacancy. It only forms a weak van der Waals bond, so it does not passivate directly.[12] However, TFSI is a strong protonating agent with a large Hammett number (H_O). Its proton (H^+) is assumed to be the passivating agent. Figure 1 shows protons leaving the TFSI anion and approaching the S vacancy. The vacancy complex with protons can trap electrons if necessary to form a local closed-shell system.

To understand the adsorption configuration, proton passivation is modeled as a function of its charge state. Unlike in Si, the bonding in MoS_2 is multi-centered. One Mo dangling bond contributes only 2/3 of an electron to a Mo-S bond, rather than one electron as in a Si-Si bond. The vacancy

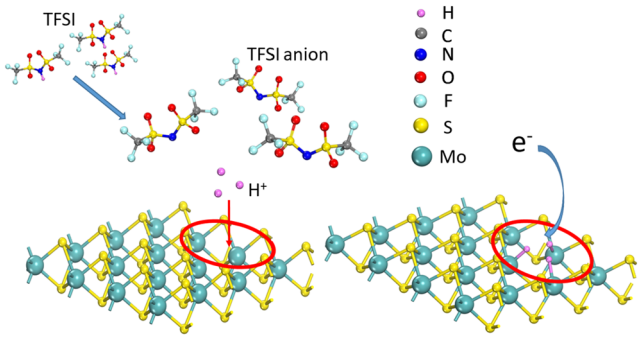

FIG. 1. TFSI passivation schematic. The super-acid is a strong protonating agent where the protons can move freely to the vacancy site and interact with Mo dangling bonds. In the figure, three Hs are adsorbed onto the S vacancy where additional electrons can be trapped. The vacancy is at the centre of the red circle.

site has trigonal C_{3v} symmetry, where three Mo dangling bonds form one resonant a_1 state and two degenerate e states around the gap, Figs. 2(a) and 2(b).[37,40]

To clean up the gap states, the symmetry should be conserved. Any half-filling of the e states breaks their spin degeneracy. Therefore, the adsorption configuration should be closed-shell with trigonal symmetry, which needs three hydrogens. DFT modeling shows that the 3-H complex can either relax into symmetrical or asymmetrical site, depending on the electron occupation of the

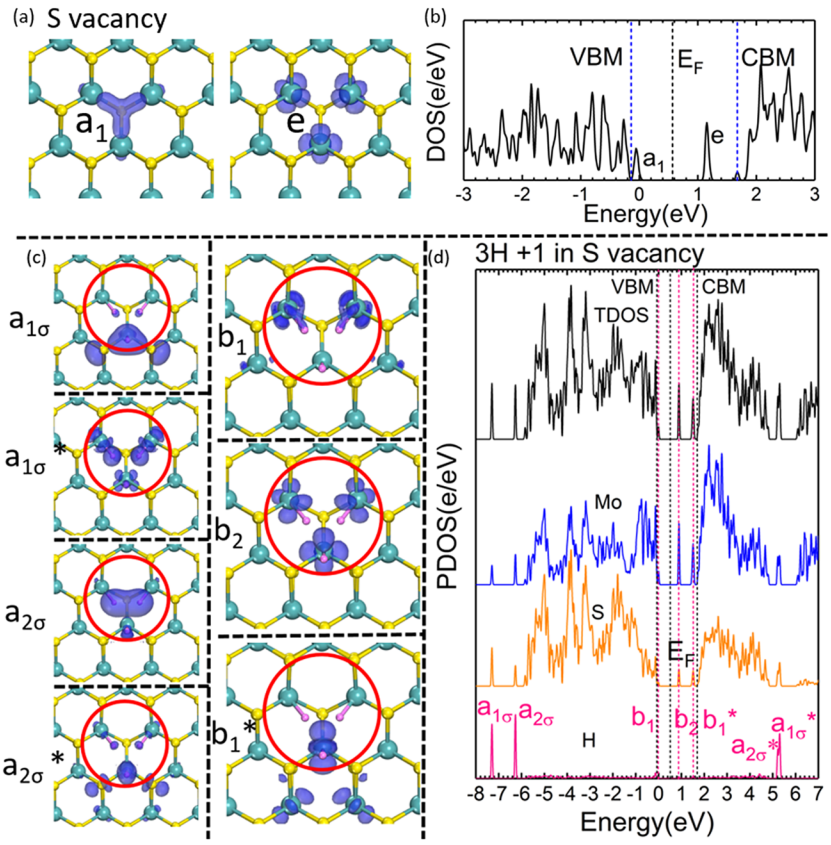

FIG. 2. Simple S vacancy (top) and passivation by 3 hydrogens in the +1 state. (a) Defect orbitals and (b) density of states of the a_1 and e gap states of the isolated S vacancy. (c) Asymmetric C_{2v} configuration for 3 protons at the vacancy with two electrons. Orbitals of the various localized states. The S vacancy lies at the centre of red circle. (d) PDOS showing the energies of the localized states.

complex. The +1 (2e) and −1 (4e) charged systems were considered by adding either 2 or 4 electrons to the system of defect with three protons.

The +1 charged system is found to relax into an asymmetric C_{2v} configuration. Here, two hydrogens stay in the defect centre, while the third hydrogen moves away to an asymmetric off-center site over a Mo atom, see Fig. 2(c). The first two H's form a filled b_1 bonding state with two of the Mo dangling bonds, Fig. 2(d). Its empty anti-bonding partner b_1^* lies in the gap just below the conduction band minimum (CBM). The second e state forms an empty b_2 state in the midgap, localized mainly on the Mo dangling bonds.

The a_1 state of the vacancy interacts with the symmetric combination of the three hydrogens to form the $a_{1\sigma}$ and $a_{1\sigma}^*$ states at −6.3 eV and 5.5 eV, respectively, well away from the bandgap, Figs. 2(d) and 3(a). The asymmetric hydrogen interacts with two sulfur atoms to form the $a_{2\sigma}$ and $a_{2\sigma}^*$ states at −7.4 eV and 5.4 eV, respectively, also well away from the bandgap. The orbital character to the $a_{2\sigma}$ state is also seen in the partial density of states (PDOS) in Fig. 2(d). The asymmetric geometry of the +1 geometry is driven by the need to keep an empty b_2 state.

There is no passivation in the +1 configuration because of its lower symmetry. The off-center hydrogen atom means that the $b_1 - b_1^*$ splitting is too small to move these states out of the bandgap, and the low symmetry and lack of interaction with hydrogens mean that the b_2 state also remains in the midgap.

To passivate all the e symmetry derived states, two more electrons should be added, giving a −1 charge (4e). Figures 4(a)–4(f) shows the energetically favorable configuration, with three identical hydrogens and C_{3v} symmetry. The hydrogen orbitals form states of a_1 and e symmetry, each of which interact with Mo dangling bond orbital combinations of the same symmetry, to form bonding states and anti-bonding states. The resulting $a_{1\sigma}$ states lie deep in the valence band at −6.30 eV, and their anti-bonding partner $a_{1\sigma}^*$ lies well above the conduction band minimum (CBM) at 5.50 eV, Figs. 3(d) and 4(b). Both of these orbitals extend along three local Mo-H bonds, Fig. 4(a). The e states also form bonding and anti-bonding states, e and e^*. The splitting of the e and e^* states is now much larger than in the +1 case, and both states lie within the bands and outside the gap, as can be seen comparing Figs. 3(a) and 3(b).

Figure 4(g) shows the PDOS of the −1 state. This configuration repairs the S vacancy in MoS_2 and preserves the direct bandgap of 1.72 eV of perfect 2D MoS_2. The highest occupied molecular orbital (HOMO) is a delocalized Mo state, derived from pure MoS_2. The e state is a local resonant state. Both of them lie below the HOMO. Therefore, all gap states are removed and E_F lies at the midgap, and the 3H/4e passivation scheme is successful. The higher symmetry of this site has caused a larger bonding-antibonding splitting of the states to remove all the gap states.

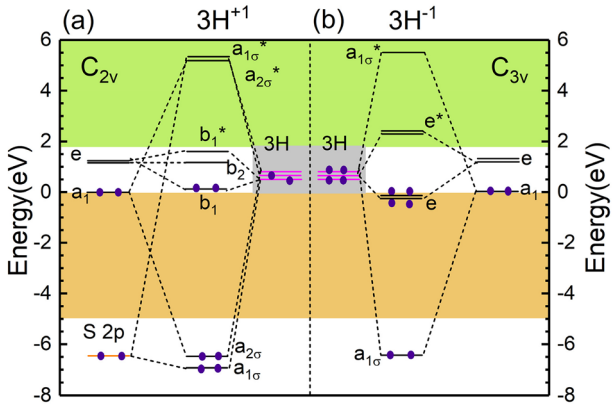

FIG. 3. Molecular orbital diagram of 3 hydrogens interacting with S vacancy states. (a) Origin of a_1, a_2, b_1, and b_2 states for the C_{2v} 2 electron, +1 configuration. Some states remain in the gap. (b) Origin of the states of a_1 and e symmetry states for the C_{3v} 4-electron, −1 configuration. The energy levels of H atoms are in violet. The valence band is in orange, and the conduction band is green. All states are repelled from the gap in the −1 charge case because its higher symmetry causes an overall larger Mo-H interaction.

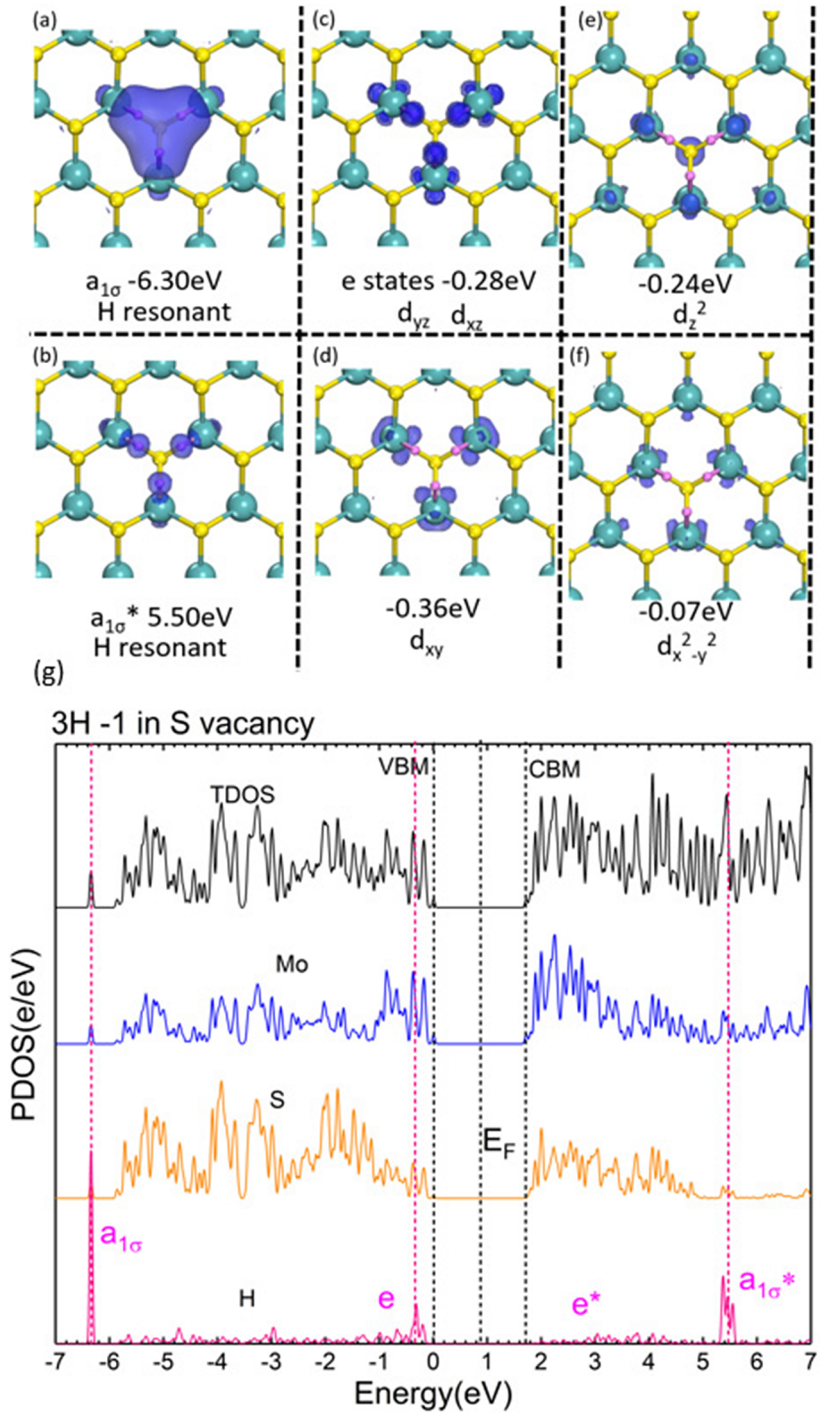

FIG. 4. Passivation by 3 hydrogens in −1 charge state. (b) Orbitals of localized states in 3H −1 passivated S vacancy with C_{3v} symmetry: (a) hydrogen resonant bonding state $a_{1\sigma}$ which is below VBM, (b) hydrogen resonant anti-bonding state $a_{1\sigma}{}^{*}$ located high in conduction bands, (c) doubly-degenerate bonding state of hydrogen with e states. Apart from hydrogen-related states, there are localized resonant states near the VBM [(d)–(f)], which are the d orbitals of the 3 adjacent Mo atoms. (g) PDOS showing various defect states.

Figure 5(a) shows the geometry for the vacancy with one hydrogen and a +1 charge state. For the 1H case, the hydrogen lies centrally in the vacancy, and this complex gives an empty state at the midgap. For the 2H case, Fig. 5(b), the hydrogens form Mo-H bonds with the dangling bonds and

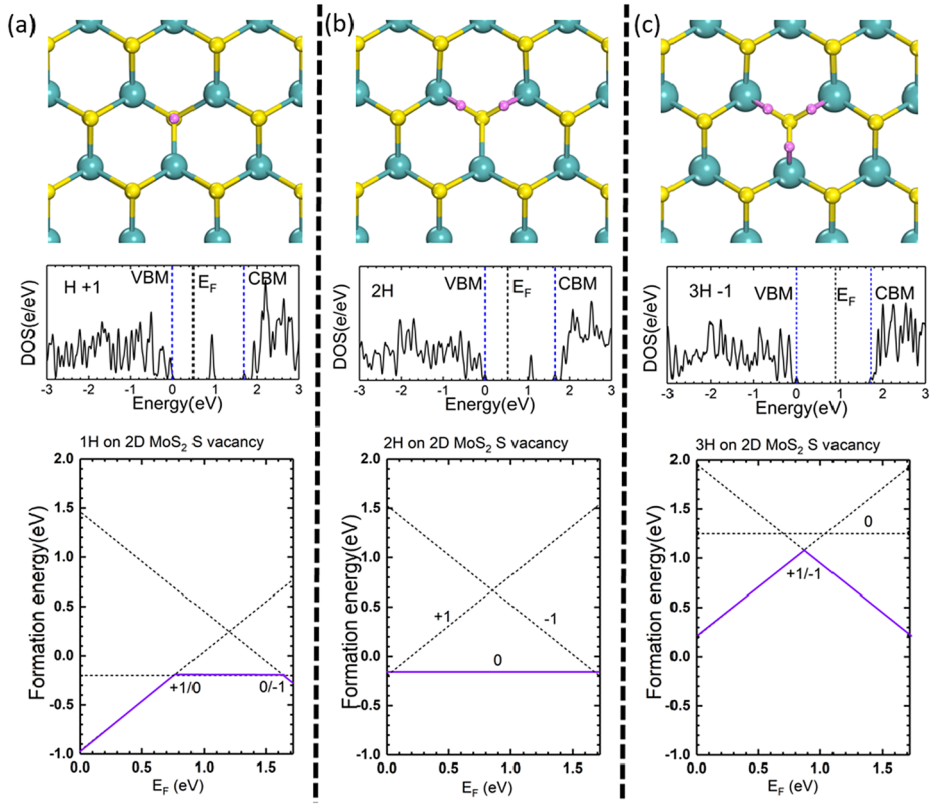

FIG. 5. [(a)–(c)] Geometry, local electronic density of states, and defect formation energy diagrams of one, two, and three hydrogens at the S vacancy in their H^+, $2H^0$, and $3H^-$ configurations. The energies are referenced to the chemical potential of the H_2 molecule.

leave a single dangling bond with no hydrogen, and it gives a midgap state. Figure 5 also shows the formation energy vs E_F for each charge state, referenced to the chemical potential of H_2. This shows that the 1H and 2H have a low formation energy. On the other hand, the 3H state has a slightly higher formation energy, but it is the only state which removes all gap states.

The function of the TFSI superacid is to supply a strongly acidic ambient to push the equilibrium toward greater binding of hydrogen with the Mo dangling bonds. TFSI raises the chemical potential of H toward that of atomic H. This can be estimated from the Hammett acidity function of superacids as measured by Kutt *et al.*,[41] as described in the Appendix, to roughly 0.5 eV in Fig. 5(c). This energy is above the stability line of the −1 state so that electrons can be attracted to the defect if E_F is above the midgap (the +1/−1 transition state), due to background impurity levels often present in *n*-type MoS_2.

Hydrogen is not as effective a passivant of the S vacancy in MoS_2 as in Si-based systems because the energetics are less favorable, and that passivation occurs in only one charge state due to the complexity and symmetry effects associated with multi-center bonding. The passivation efficiency is reduced by the ability of hydrogens to recombine into molecular hydrogen due to the ability of Mo-rich plane edge sites and S vacancy sites to catalyse the hydrogen evolution reaction—which is favored by only weak H binding energy.[42,43]

Hydrogen also binds to basal plane S sites, with the on-top site being the most stable. It is however 1.1 eV less stable than at the S vacancy. The H can hop via the hollow site to an adjacent on-top site, with an energy barrier of only 0.1 eV. In this way, protons donated by TFSI are able to diffuse and find S vacancy sites.

We also consider other passivation methods. By analogy to passivation of the O vacancy in HfO_2, we can use two substitutional acceptors near the vacancy to compensate the loss of one S atom, and to give the correct number of valence electrons to make a closed shell configuration, and return E_F to

the midgap.[44,45] This causes the vacancy to become V^{2+}. This charge causes a strong ionic relaxation around the vacancy which repels the vacancy state above the CBM and so clears the gap of defect states. In MoS_2, the process involves either replacing two Mo atoms with two Nb atoms, or replacing two adjacent S atoms with two As atoms, as in Figs. 6(a) and 6(b). Figure 6(a) shows the atomic configuration and defect orbitals of Nb_{Mo} schemes. There are three different defect states, a_1: the asymmetrical resonant state, b_1: the d orbital of the local Mo hybrid with the Nb resonant state, and b_2: the d orbital of the local Mo and Nb, Fig. 6(b). However, unlike the case of HfO_2, the a_1 vacancy state lies at the bottom of the gap, so E_F of the modified system lies at the VB edge.

This scheme fails to passivate because the b_1 and b_2 defect states do not move out of the gap. Despite its formal ionic charge of Mo^{+4}, the Mo-S bond in MoS_2 is not very ionic. The Bader charge of Mo in MoS_2 is actually only +0.22. Thus there is little ionic relaxation of Mo sites toward the positive vacancy as there was in HfO_2 to move the b_2 state out of the gap. Therefore, substitutional doping does not passivate the S vacancy.

The oxygen O_2 molecule is known to passivate the S vacancy experimentally. It is thought to occur by adding the undissociated O_2 molecule across the vacancy. The isolated neutral O_2 molecule is a spin triplet with two electrons with the same spin lying in the π_{px}^* and π_{py}^* states. Although the most stable configuration of molecular O_2 is open-shell, it becomes close-shell when chemisorbed onto the S vacancy. As an undissociated molecule, one atom, O_1, forms two Mo—O bonds and its second oxygen atom O_2 forms one Mo—O bond. The three Mo—O bonds have the same length, 2 Å, which allows O_1 to lie inside the monolayer, while atom O_2 stays outside the monolayer, as in the side view in Fig. 6(a). This adsorption configuration is energetically stable after overcoming an energy barrier at room temperature.[22] The passivation occurs by compensating the S vacancy with the two unpaired π electrons from O_2. Bader charge analysis shows that charge is distributed evenly over the three Mo's, while O_2 is more slightly electronegative than O_1. Figure 6(a) shows the oxygen hybrid a_1 and e states. Breaking the trigonal symmetry, the e states split up into b_1 and b_2 states, as shown in Fig. 6(b). The a_1 state is an oxygen state near the VBM, lying just in the gap. The b_1 and b_2 states are in the conduction band.

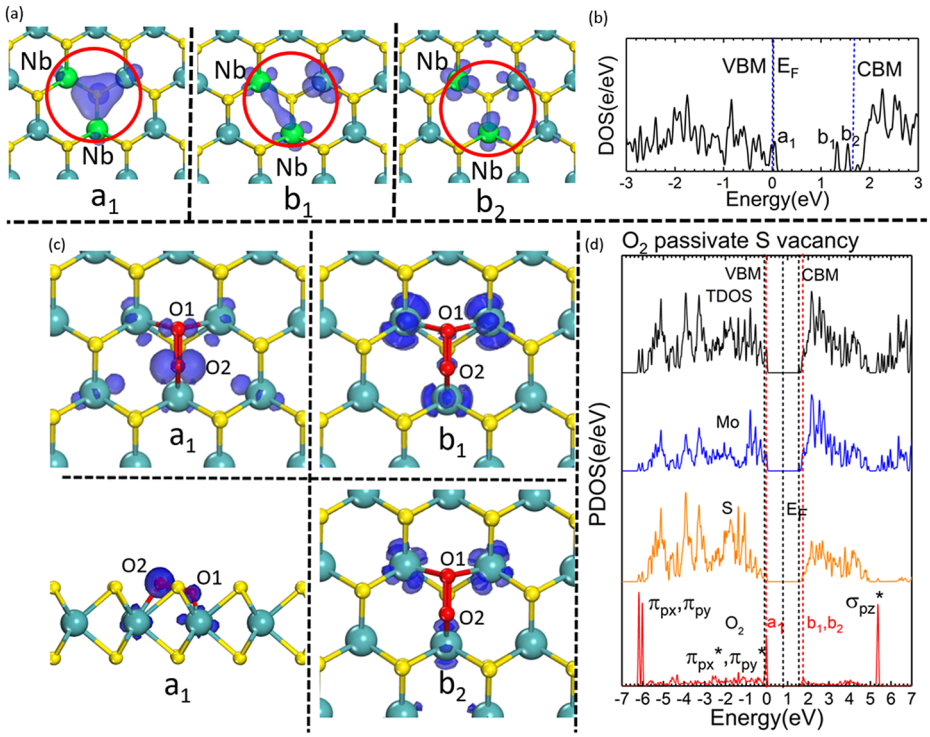

FIG. 6. [(a) and (b)] Attempted passivation of S vacancy by two adjacent Nb_{Mo} sites, showing orbitals and PDOS. [(c) and (d)] Passivation of S vacancy by an O_2 molecule lying across the vacancy, orbitals and PDOS.

Despite the obvious advantage of the oxygen scheme which only needs neutral oxygen, the symmetry is broken, which means that the gap states are not sufficiently moved into the VB or CB. However, the a_1 state is fully occupied by four electrons as shown, so the vacancy is not a charge trap center. The S vacancy may already be partially passivated during the growth of 2D MoS_2 since it is exposed to air. It is possible that increasing the oxygen density or raising the temperature to help O_2 over the adsorption energy barrier may achieve better passivation.

Atomic oxygen will also passivate the S vacancy, being 2.1 eV more stable than adding S. Atomic O could be produced by a plasma or ozone. However, care would need to be taken that MoS_2 is not oxidized too far to an Mo oxide.

In summary, we investigated the electronic properties of S vacancy and possible passivation schemes. Three hydrogen atoms symmetrically adsorbed around the S vacancy site in its −1 charge state successfully remove all gap states and return E_F to the midgap. The passivation mechanism is more complex than of covalently bonded systems like Si and SiO_2 because of the multi-centered bonding in MoS_2 and the resulting symmetry constraints that this imposes. Symmetry is critical to moving the defect states out of gap, to avoid lifting the defect state degeneracy, and because a sufficient energy splitting of bonding and anti-bonding states is needed to move states completely out of the gap. Other methods such as substitutional doping are not as effective because, for example, the Mo—S bond is not as ionic as HfO_2.

The authors acknowledge funding from EPSRC Grant No. EP/P005152/1 and CSC. The authors are also grateful to A. Javey for drawing attention to Ref. 41.

APPENDIX: ANALYSIS OF PROTON CHEMICAL POTENTIAL DUE TO TFSI

The Hammett acidity function (H_O) allows the calculation of the ratio of the real concentration of the base (B) and superacid (BH^+) in solution if you know the pK_a (called pK_{BH+}). Normally all you can calculate from the pK_a are the activities. The activity (a) is the product of the mole fraction (x) and the activity coefficient (γ). In solutions, often $a_B = \gamma_B C_B$ is used, where C_B is the molarity. Once you know the H_O, you can calculate the proton activity if you know the activity coefficients of the acid and base. In a concentrated solution, the proton activity coefficients can be far from unity,

$$H_O = pK_{BH^+} + \log([B])/[BH^+], \quad H_O = -\log(a_{H^+}\gamma_B/\gamma_{BH^+}), \quad a_B = x_B \cdot \gamma_B.$$

The chemical potential (μ) in an ideal solution is the chemical potential of the pure substance (μ^0) plus a correction proportional to the log of the mole fraction (x). However, in a real solution the chemical potential is equal to the chemical potential of the pure substance plus a correction proportion to log(a). However the activity is a function of the concentration, (especially in a concentrated solution) so it must be measured. Therefore, there is no easy way to calculate the chemical potential from H_O,

$$\mu_B = \mu_B{}^0 + RT\ln(x_B), \quad \mu_B = \mu_B{}^0 + RT\ln(a_B).$$

To work around this, Kutt[41] developed a method to quantify protonation strength to the solvents (DCE and MeCN) and make measurements on 66 superacids. In solutions of DCE, the TFSI $(CF_3SO_2)_2NH$ (denoted as HA), will partially protonate DCE denoted as S (solvent). The pK_a value gives the relative amount of protonated solvent in dilute solution,

$$HA + S \leftrightarrow A^- + SH^+, \quad pK_a = -\log a(SH^+) \cdot a(A^-)/a(HA).$$

For TFSI, K_a(DCE) is −11.9, while K_a(MeCN) = 0.3; they are about 9.4 points lower than the values for H_2SO_4 [Ka = −2.5 (DCE) and 8.7 (MeCN)], a common reference. Therefore, although one cannot calculate the chemical potential of TFSI, one can say it is likely to raise the chemical potential of the proton donating species (SH+) by $RT\ln(10^{-pKa})$ which at 25 C equals ~0.50 eV.

[1] K. F. Mak, C. Lee, J. Hone, J. Shan, and T. F. Heinz, Phys. Rev. Lett. **105**, 136805 (2010).
[2] K. F. Mak and J. Shan, Nat. Photonics **10**, 216 (2016).
[3] D. Jariwala, V. K. Sangwan, L. J. Lauhon, T. J. Marks, and M. C. Hersam, ACS Nano **8**, 1102 (2014).
[4] B. Radisavljevic, A. Radenovic, J. Brivio, V. Giacometti, and A. Kis, Nat. Nanotechnol. **6**, 147 (2011).
[5] Y. Yoon, K. Ganapathi, and S. Salahuddin, Nano Lett. **11**, 3786 (2011).
[6] D. Sarkar, X. Xie, W. Liu, W. Cao, J. Kang, Y. Gong, S. Kraemer, P. M. Ajayan, and K. Banerjee, Nature **526**, 91 (2015).

[7] C. Gong, H. J. Zhang, W. H. Wang, L. Colombo, R. M. Wallace, and K. J. Cho, Appl. Phys. Lett. **103**, 053513 (2013).
[8] W. Zhou, X. Zou, S. Najmaei, Z. Liu, Y. Shi, J. Kong, J. Lou, P. M. Ajayan, B. I. Yakobson, and J. C. Idrobo, Nano Lett. **13**, 2615 (2013).
[9] J. Hong, Z. Hu, M. Probert, K. Li, D. Lv, X. Yang, L. Gu, N. Mao, Q. Feng, L. Xie, J. Zhang, D. Wu, Z. Zhang, C. Jin, W. Ji, X. Zhang, J. Yuan, and Z. Zhang, Nat. Commun. **6**, 6293 (2015).
[10] X. Zou, Y. Liu, and B. I. Yakobson, Nano Lett. **13**, 253 (2013).
[11] S. Najmaei, Z. Liu, W. Zhou, X. L. Zou, G. Shi, S. D. Lei, B. I. Yakobson, P. M. Ajayan, and J. Lou, Nat. Mater. **12**, 754 (2013).
[12] M. Amani, D. Lien, D. Kiriya, J. Xiao, A. Azcatl, J. Noh, S. R. Madhvapathy, R. Addou, S. Kc, M. Dubey, K. Cho, R. M. Wallace, S. Lee, J. He, J. W. A. Iii, X. Zhang, E. Yablonovitch, and A. Javey, Science **350**, 1065 (2015).
[13] K. Kaasbjerg, K. S. Thygesen, and K. W. Jacobsen, Phys. Rev. B **85**, 115317 (2012).
[14] A. Allain, J. Kang, K. Banerjee, and A. Kis, Nat. Mater. **14**, 1195 (2015).
[15] J. H. Park, A. Sanne, Y. Guo, M. Amani, K. Zhang, H. C. P. Movva, J. A. Robinson, A. Javey, J. Robertson, S. K. Banerjee, and A. C. Kummel, Sci. Adv. **3**, e1701661 (2017).
[16] Z. Yu, Y. Pan, Y. Shen, Z. Wang, Z.-Y. Ong, T. Xu, R. Xin, L. Pan, B. Wang, L. Sun, J. Wang, G. Zhang, Y. W. Zhang, Y. Shi, and X. Wang, Nat. Commun. **5**, 5290 (2014).
[17] M. Makarova, Y. Okawa, and M. Aono, J. Phys. Chem. C **116**, 22411 (2012).
[18] K. Cho, M. Min, T. Y. Kim, H. Jeong, J. Pak, J. K. Kim, J. Jang, S. J. Yun, Y. H. Lee, W. K. Hong, and T. Lee, ACS Nano **9**, 8044 (2015).
[19] D. M. Sim, M. Kim, S. Yim, M. J. Choi, J. Choi, S. Yoo, and Y. S. Jung, ACS Nano **9**, 12115 (2015).
[20] H. Nan, Z. Wang, W. Wang, Z. Liang, Y. Lu, and Z. H. Ni, ACS Nano **8**, 5738 (2014).
[21] P. K. Gogoi, Z. Hu, Q. Wang, A. Carvalho, D. Schmidt, X. Yin, Y. H. Chang, L. J. Li, C. H. Sow, A. H. C. Neto, M. B. H. Breese, A. Rusydi, and A. T. S. Wee, Phys. Rev. Lett. **119**, 077402 (2017).
[22] Y. Liu, P. Stradins, and S.-H. Wei, Angew. Chem., Int. Ed. **55**, 965 (2016).
[23] M. Amani, R. A. Burke, X. Ji, P. Zhao, D. H. Lien, P. Taheri, G. H. Ahn, D. Kirya, J. W. Ager, E. Yablonovitch, J. Kong, M. Dubey, and A. Javey, ACS Nano **10**, 6535 (2016); H. Kim, D. H. Lien, M. Amani, J. W. Ager, and A. Javey, *ibid.* **11**, 5179 (2017).
[24] Y. Yu, G. Li, L. Huang, A. Barrette, Y. Q. Cai, Y. Yu, K. Gundogdu, Y. W. Zhang, and L. Cao, ACS Nano **11**, 9390 (2017).
[25] A. Alharbi, P. Zahl, and D. Shahrjerdi, Appl. Phys. Lett. **110**, 033503 (2017).
[26] K. L. Brower and S. Myers, Appl. Phys. Lett. **57**, 162 (1990).
[27] A. H. Edwards, Phys. Rev. B **44**, 1832 (1991).
[28] J. H. Stathis and E. Cartier, Appl. Phys. Lett. **63**, 1510 (1993).
[29] C. J. Sandroff, R. N. Notenburg, J. C. Bischoff, and R. Bhat, Appl. Phys. Lett. **51**, 33 (1987).
[30] M. Radosavjevic *et al.*, *Tech Digest IEDM* (IEEE, 2009), p. 13.1.
[31] L. Lin and J. Robertson, App. Phys. Lett. **98**, 082903 (2011).
[32] S. J. Clark, M. D. Segall, C. J. Pickard, P. J. Hasnip, M. I. J. Probert, K. Refson, and M. C. Payne, Z. Kristallogr.–Cryst. Mater. **220**, 567 (2005).
[33] S. J. Clark and J. Robertson, Phys. Rev. B **82**, 085208 (2010).
[34] S. Grimme, J. Comput. Chem. **27**, 1787 (2006).
[35] S. Lany and A. Zunger, Phys. Rev. B **78**, 235104 (2008).
[36] P. A. Young, J. Phys. D: Appl. Phys. **1**, 936 (1968).
[37] D. Liu, Y. Guo, L. Fang, and J. Robertson, Appl. Phys. Lett. **103**, 183113 (2013).
[38] H. Lu and J. Robertson, Appl. Phys. Lett. **112**, 062105 (2017); Y. Guo and J. Robertson, Phys. Rev. Mater. **1**, 044004 (2017).
[39] S. N. Suarez, J. R. P. Jayakody, S. G. Greenbaum, T. Zawodzinski, and J. J. Fontanella, J. Phys. Chem. B **114**, 8941 (2010).
[40] J. Y. Noh, H. Kim, and Y. S. Kim, Phys. Rev. B **89**, 205417 (2014).
[41] A. Kutt, T. Rodima, J. Saame, E. Raamat, V. Maemats, I. Kaljiurand, I. A. Koppel, R. Y. Garlyauskayte, Y. L. Yagupolskii, L. M. Yagupolskii, E. Bernhardt, H. Willner, and I. Leite, J. Org. Chem. **76**, 391 (2011).
[42] C. Tsai, F. Abild-Pedersen, and J. K. Nørskov, Nano. Lett. **14**, 1381 (2014).
[43] H. Li, C. Tsai, A. L. Koh, L. Cai, A. W. Contryman, A. H. Fragapane, J. Zhao, H. S. Han, H. C. Manoharan, F. Abild-Pedersen, J. K. Nørskov, and X. Zheng, Nat. Mater. **15**, 48 (2016).
[44] K. Xiong, J. Robertson, and S. J. Clark, J. Appl. Phys. **99**, 044105 (2006).
[45] D. Liu and J. Robertson, Appl. Phys. Lett. **94**, 042904 (2009).